JOURNAL OF MATERIALS SCIENCE 31 (1996) 4725–4740

Statistical analysis of porosity in Al–9 wt %Si–3 wt %Cu–*X* alloy systems

N. ROY, P. R. LOUCHEZ, F. H. SAMUEL
Département des Sciences appliquées, Université du Québec à Chicoutimi, Chicoutimi (Québec), G7H 2B1 Canada

A set of 72 solidification experiments was carried out on Al–9 wt %Si–3 wt %Cu–*X* alloys, varying the additives (namely, strontium, grain refiner and other alloying elements), hydrogen level and thermal parameters in order to obtain a statistical analysis of the resulting porosity in such alloy systems. For all the cases studied, it was found that in each case, the smaller sized pores (in terms of pore length or pore area) could be described by an exponential function, while the larger sized pores were distributed in an irregular fashion, "small" and "large" being distinguished by that limiting value of pore length or area at which the average value equalled the standard deviation. Two different approaches i.e. factorial and regression methods were utilized to quantify the importance of the parameters controlling the pore size and porosity volume fraction. Two main observations were made: (i) hydrogen is the strongest parameter enhancing porosity formation, with the hydrogen–grain refiner, strontium, strontium–titanium and solidus velocity–solidification time interactions being the other parameters that contribute significantly to porosity formation and increase in pore size; (ii) the grain refiner, hydrogen–phosphorus, strontium–magnesium and iron–phosphorus interaction parameters reduce the porosity, though in different magnitudes. The reliability of predicting the observed effects by the two methods has been discussed.

1. Introduction

Huang and Berry [1] have classified the porosity in aluminium castings into two kinds: (i) macroporosity, comprising mainly of massive shrinkage cavities and occurring in long-freezing range alloys, caused by failure to compensate for solidification shrinkage; and (ii) dispersed pores or microporosity due to the failure to feed the interdendritic regions, and the precipitation of dissolved gases. The latter kind, invariably found in most aluminium alloy castings, is a consequence of the influence of several strongly interacting alloy and process parameters that determine the amount and nature of porosity that will occur in a casting [2]. As such porosity is known to significantly influence the mechanical properties, it becomes essential to quantify microporosity formation as a function of these parameters, particularly in the case of castings used in critical structural applications, where it is important to be able to predict the occurrence of the porosity with reasonable accuracy.

According to Tynelius *et al.* [2], the many investigations on porosity in aluminium castings can be divided into two main categories. The first category includes works that experimentally investigate the amount and size of macroporosity using one or more distinctly shaped test moulds [3–8]. The second category includes studies aimed at an understanding of the formation of porosity through mathematical modelling. Some of the studies covering this category are those of Walther *et al.* [9] on single centreline pores in cylinders of pure Mg and Al under constant radial heat extraction conditions, and similar studies by Fredriksson and Svensson [10] on stainless steel under directional solidification conditions; that of Shahani [11] on pore length in pure aluminium; and those of various authors on volume per cent porosity and pore size in Al–4.5% Cu [12, 13], A356.2 [14, 15] and Al–7% Si [16] alloys.

Statistical data reduction techniques are usually adopted in the quantitative prediction of porosity in such aluminium alloy castings. Factorial and multiple regression analysis methods are typical of such techniques.

In the case of A356 alloy, one of the more popular commercial casting alloys belonging to the Al–Si system, many investigations have been carried out to evaluate the effect of solidification parameters, grain refinement and modification on porosity evolution in this alloy under directional solidification conditions. In particular, those of Fang and Granger [14] and Tynelius [17] have shown that:

(a) Hydrogen and strontium contents significantly increase the pore volume fraction and pore size. Their effect decreases with increased cooling rate.
(b) Grain refining reduces both pore volume fraction and pore size. It also promotes a more uniform distribution of pores.

0022–2461

(c) A higher cooling rate gives a higher threshold hydrogen content, a level at which a certain residual pore volume fraction occurs. Strontium (Sr) modification (i.e. an increase in the Sr level of the alloy) and an increase in solidus velocity both decrease the threshold hydrogen limit.

The present study was undertaken to demonstrate the effect of hydrogen content, additives, and thermal parameters on the pore size and porosity volume fraction obtained in Al–Si–Cu alloy systems. Based on the experimentally obtained data, the quantity and size of pores could be predicted using statistical methods namely, factorial and multiple regression methods.

Examples of the porosity features typically observed in alloy samples studied in the present work, as well as the definitions of the various porosity parameters measured are given in Appendix 1.

2. Experimental procedure

The base alloy containing Al–6 wt % Si–3 wt % Cu–0.15 wt % Fe was prepared from pure elements, and supplied in the form of 12.5 kg ingots. The final composition was adjusted by adding Al–*X* master alloys, except in the case of Si, which was added in the form of pure metal (containing 15 p.p.m. calcium). Table I shows the compositions that were aimed for, whereas Table II lists the chemical compositions that were obtained for the alloys used in the present work. The latter were determined from inductive couple plasma (ICP) analysis, carried out at Alcan's Arvida Research and Development Centre, Jonquière, Québec, Canada.

The alloys were melted in a silicon carbide crucible of 7 kg capacity using an electrical resistance furnace. The melting temperature was adjusted at 735 ± 5 °C. Two tapered variable angle wedge-shaped metallic moulds were employed, one kept at an opening angle of 5° and heated at 40 °C (to avoid moisture pick-up) (Fig. 1(a)) and the other kept at 15 °C heated at 300 °C (Fig. 1(b)). The inner surfaces of both moulds were coated with a thin layer of vermiculite to facilitate removal of the castings. Prior to casting, the moulds were inclined at 35° with respect to the vertical position, and then tilted up during pouring to minimize turbulence effects.

The melt hydrogen level was monitored using an AlScan™ unit, one of the commercial techniques available for direct measurements of the melt hydrogen content. The AlScan apparatus is based on the Telegas or the "closed-loop recirculation" technique developed by Ransley and co-workers [18] to measure the partial pressure of hydrogen in molten aluminium. The underlying principle is to create a circulating gas volume (of nitrogen gas) within the molten metal into which hydrogen can diffuse. The inert gas is bubbled through the melt and collected by an inverted bell-shaped ceramic probe. After a reasonable time, the dissolved hydrogen in the melt attains an equilibrium with the hydrogen gas contained in the nitrogen bubbles. The concentration of hydrogen in solution is calculated as a function of its solubility (at a given temperature and 760 mmHg pressure) and partial pressure. Operation of the instrument is simple with the preselection of a specific number of parameters including an alloy correction factor [19].

In addition to the on-line measurements of hydrogen using the AlScan™, specimens were also cast simultaneously in a Ransley mould (for each pouring/casting) from which "Ransley" samples were

TABLE I Aimed compositions (wt %) and hydrogen levels (ml/100 g Al) for the alloys prepared for the present work

Alloy	Zn	Fe	Mg	Mn	Ti	Sr	P	GR[a] (Ti)	H	Si	Cu
f1	0	0.1	0.35	0	0.13	0.015	0	0.02	0.25	9	3
f2	0	0.1	0.35	0.6	0.13	0.015	0.006	0.02	0.25	for	for
f3	0	1.0	0.35	0	0.13	0.015	0.006	0.02	0.25	all	all
f4	0	1.0	0.35	0.6	0.13	0.015	0	0.02	0.25	alloys	alloys
f5	3	0.1	0.35	0	0.13	0.015	0.006	0.02	0.25		
f6	3	0.1	0.35	0.6	0.13	0.015	0	0.02	0.25		
f7	3	1.0	0.35	0	0.13	0.015	0	0.02	0.25		
f8	3	1.0	0.35	0.6	0.13	0.015	0.006	0.02	0.25		
h1	1.5	0.55	0	0.3	0.13	0.015	0	0	0.1		
h2	1.5	0.55	0	0.3	0.13	0.015	0	0.02	0.4		
h3	1.5	0.55	0	0.3	0.13	0.015	0.006	0	0.4		
h4	1.5	0.55	0	0.3	0.13	0.015	0.006	0.02	0.1		
h5	1.5	0.55	0.7	0.3	0.13	0.015	0	0	0.4		
h6	1.5	0.55	0.7	0.3	0.13	0.015	0	0.02	0.1		
h7	1.5	0.55	0.7	0.3	0.13	0.015	0.006	0	0.1		
h8	1.5	0.55	0.7	0.3	0.13	0.015	0.006	0.02	0.4		
s1	0	0.55	0	0.3	0	0	0.003	0.02	0.25		
s2	0	0.55	0	0.3	0.25	0.030	0.003	0.02	0.25		
s3	0	0.55	0.7	0.3	0	0.030	0.003	0.02	0.25		
s4	0	0.55	0.7	0.3	0.25	0	0.003	0.02	0.25		
s5	3	0.55	0	0.3	0	0.030	0.003	0.02	0.25		
s6	3	0.55	0	0.3	0.25	0	0.003	0.02	0.25		
s7	3	0.55	0.7	0.3	0	0	0.003	0.02	0.25		
s8	3	0.55	0.7	0.3	0.25	0.030	0.003	0.02	0.25		

[a] GR = grain refiner (Al–5 wt % Ti–1 wt % B).

TABLE II Actual compositions (wt %) of the cast alloys used in the present work (obtained from ICP analysis)

Alloy	Si	Cu	Zn	Fe	Mg	Mn	Ti	Sr	P
f1	8.93	3.08	0.01	0.22	0.32	0	0.14	0.013	0
f2	for	3.18	0.01	0.16	0.35	0.6	0.15	0.023	0.0019
f3	all	3.19	0.10	1.19	0.31	0	0.15	0.090	0
f4	alloys	3.31	0.06	1.06	0.33	0.62	0.14	0.022	0
f5		3.23	0.7	0.19	0.29	0	0.137	0.012	0.0033
f6		2.77	0.7	0.19	0.28	0.6	0.148	0.014	0
f7		2.78	0.8	1.0	0.28	0	0.11	0.014	0
f8		2.94	1.13	0.95	0.27	0.6	0.14	0.015	–
h1		3.02	1.48	0.54	0.08	0.35	0.13	0.024	0
h2		3.32	1.51	0.60	0.09	0.20	0.19	0.022	0
h3		3.06	1.49	0.55	0.08	0.30	0.13	0.017	0.0030
h4		3.05	1.47	0.55	0.08	0.28	0.14	0.017	0.0033
h5		2.98	1.50	0.55	0.66	0.29	0.13	0.024	–
h6		3.41	1.56	0.57	0.77	0.26	0.19	0.024	0
h7		3.68	1.56	0.57	0.61	0.36	0.14	0.017	0.0037
h8		3.12	1.47	0.53	0.66	0.30	0.19	0.027	0.0011
s1		3.40	0	0.57	0.02	0.3	0.04	0.002	0.0020
s2		3.16	0	0.56	0.01	0.3	0.27	0.043	0.0025
s3		3.06	0	0.43	0.33	0.31	0.05	0.042	0.0025
s4		3.35	0	0.53	0.24	0.3	0.29	< 0.002	0.0025
s5		2.84	1.8	0.56	0.01	0.31	0.03	0.030	0.0025
s6		2.90	1.9	0.79	0.01	0.31	0.09	< 0.002	0.0025
s7		3.16	1.7	0.54	0.67	0.3	0.03	< 0.002	0.0025
s8		2.87	1.8	0.97	0.30	0.3	0.06	0.038	0.0025

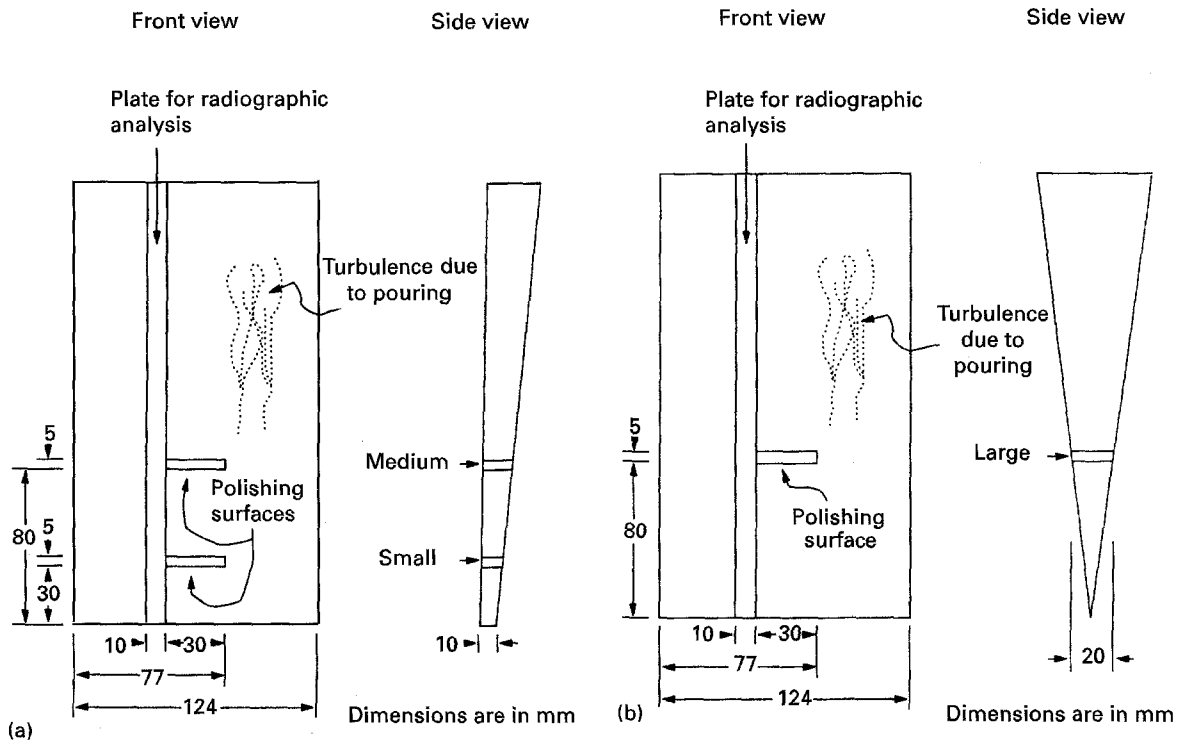

Figure 1 (a) Schematic diagram of cold mould. (b) Schematic diagram of hot mould.

machined for determination of the hydrogen content employing the Leco vacuum fusion technique. This is one of the standard methods for obtaining accurate analysis of the hydrogen content in a melt [20]. The Ransley mould (described in detail elsewhere [21]) is a copper mould originally invented by Ransley and his co-workers to produce samples for measuring the hydrogen content of a melt from the solidified casting using a standard vacuum fusion technique (like the Leco technique). Table III lists the hydrogen concentrations obtained from Leco analysis of the alloy samples. These were the values that were employed in the numerical calculations.

The porosity was quantified using a Leco 2001 image analyser, in conjunction with an optical microscope (Olympus PMG3). As shown in Fig. 1, three samples termed small (S), medium (M), and large (L) were cut from each casting, and their upper surfaces

TABLE III Hydrogen measurements (ml/100 g Al)

Alloy	H_2	Alloy	H_2
f1	0.22	h5	0.57
f2	0.25	h6	0.12
f3	0.20	h7	0.13
f5	0.25	h8	0.45
f6	0.31	s1	0.28
f7	0.31	s2	0.24
f8	0.25	s4	0.23
h1	0.06	s5	0.26
h2	0.52	s6	0.21
h3	0.49	s7	0.21
h4	0.13	s8	0.29

polished for measurements of porosity. Measurements were performed on these polished surfaces at a magnification of 50×, so as to cover the entire sample surface. As the details involved in the measurement of porosity using the image analyser have been described at length elsewhere [22], only the salient features will be mentioned here in passing. The accuracy of pore size and pore density measurements using image analysis depends on four parameters: focus, illumination, grey level, and the number of images analysed per sample. Taking into account the size of the sample (small versus medium versus large), an appropriate number of fields required to cover the entire surface was chosen at the magnification of 50× in each case, where image readings from the outer edges of the sample were discarded to avoid cooling rate discrepancies near the sample edges (in contact with the mould inner surface) compared to that at its centre.

3. Results and discussion

3.1. Thermal analysis

K-type, chromel–alumel thermocouple pairs spaced 5 mm apart were placed at the same levels at which the metallographic samples were to be cut. Fig. 2 shows the temperature–time cooling curves obtained from the three sample positions corresponding to small, medium and large as shown in Fig. 1, where the initial changes in mould temperature are superimposed. In all the curves examined, the solidification temperature of the (Al + Al_2Cu) eutectic phase was indistinguishable. Thus, based on our earlier work [23] on 380 alloy, the solidus temperature was taken to be 500 °C.

In order to calculate the thermal gradient and solidification rate, cooling curves obtained from each pair of thermocouples, as for example that shown in Fig. 2(b), were analysed as exemplified in Fig. 2(c). The results are listed in Table IV.

3.2. Porosity measurements

In order to reduce the number of experiments required for the study, three independent elements dominating the formation of porosity were selected namely, hydrogen (H), strontium (Sr) and iron (Fe). Their interactive effects with the other elements were then considered, according to the strength of the interaction. This led to the interaction parameters H–P, H–Mg,

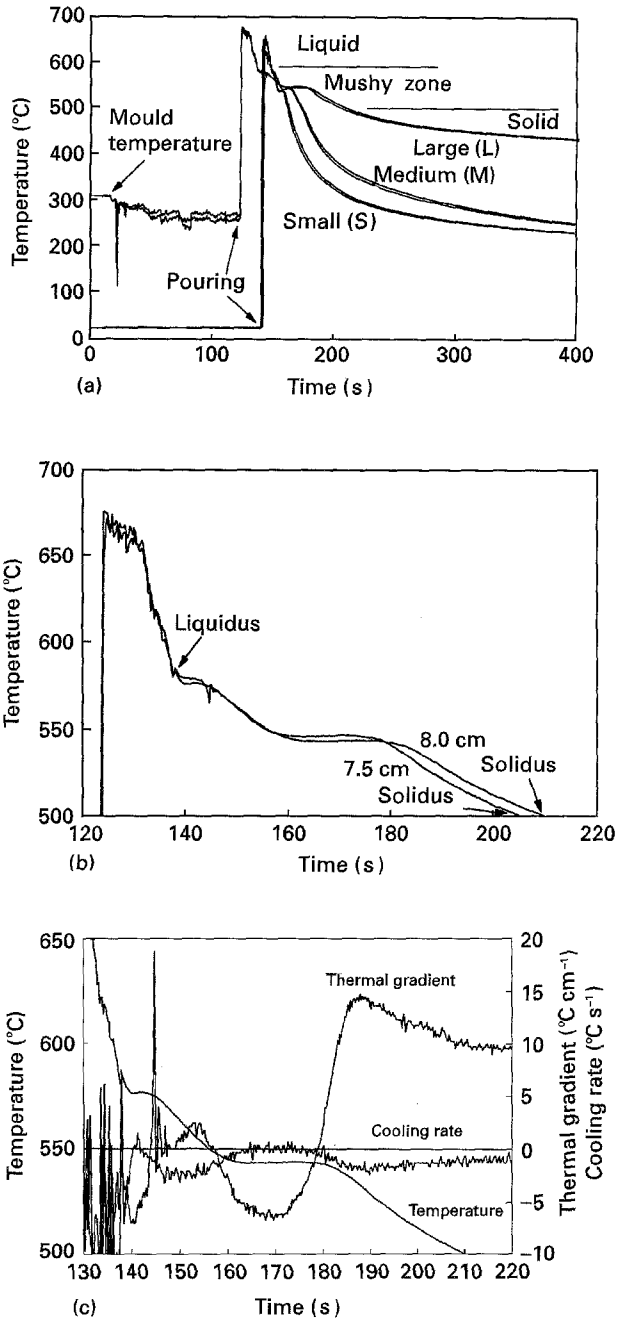

Figure 2 (a) General view of temperature–time curves obtained for the three specimen types, large, medium and small, shown in Fig. 1. Various stages of solidification for the large sample are indicated in the figure. (b) Temperature–time curve for large specimen, employing a pair of thermocouples. (c) Thermal variants obtained from temperature–time curves for large sample.

TABLE IV Solidification parameters for the small, medium and large alloy samples obtained from each casting

Specimen	Thermocouple position[a] (cm)	Solidification time, t_s (s)	Solidus velocity, V_s (cm s^{-1})
Small (S)	3.5 3.0	12.5	0.45
Medium (M)	8.0 7.5	25.2	0.36
Large (L)	8.0 7.5	70.9	0.114

[a] Height as measured from the bottom of the mould.

and H–GR (GR representing the grain refining agent Al–Ti–B, and P and Mg, phosphorus and magnesium, respectively) for the hydrogen-related interactions, Fe–Mn and Fe–P for the iron-related interactions, and Sr–Mg and Sr–Ti for the strontium-related ones (with Mn and Ti representing manganese and titanium). The Mn–P and Mg–Ti interaction parameters, which were considered equally strong, were classified as part of the iron and strontium groups, respectively. Following this method, three groups of elements/interactions were classified, each group containing a total of seven element or interaction parameters, where zinc, which does not interact with any other element, was added to both the iron and strontium groups in order to obtain the same total of seven parameters in each group. The experimental study thus covered three groups of eight alloys each (designated f, h and s for iron, hydrogen and strontium, respectively in the tables); there were 24 alloys in all.

For a given specimen, the distribution of pores in terms of the pore density (measured by the number of pores per square centimetre) versus pore length or pore area is shown in Fig. 3(a) and (b), respectively. In each case, the curve can be divided into two parts: one part representing small pores (the exponential part marked I in Fig. 3(a)), and the second comprising the large pores (the irregular part marked II in Fig. 3(a)).

For the probability function of an exponential distribution, the average of pore length or pore area (μ) must be equal to the standard deviation (σ). Thus, the limit that separates the two parts is determined by calculating μ and σ for different pore lengths, l. The pore length limit, l_{lim}, is found when μ is equal to σ. In the case of the sample shown in Fig. 3(a), the pores are divided as small and large according as their pore lengths are <95 μm or >95 μm, respectively. Fig. 4 magnifies the exponential part of the pore length distribution curve shown in Fig. 3(a) in greater detail.

The theoretical probability [24, 25], for an exponential distribution of pores can be expressed as

$$f(l) = \theta e^{-\theta l} \quad (1)$$

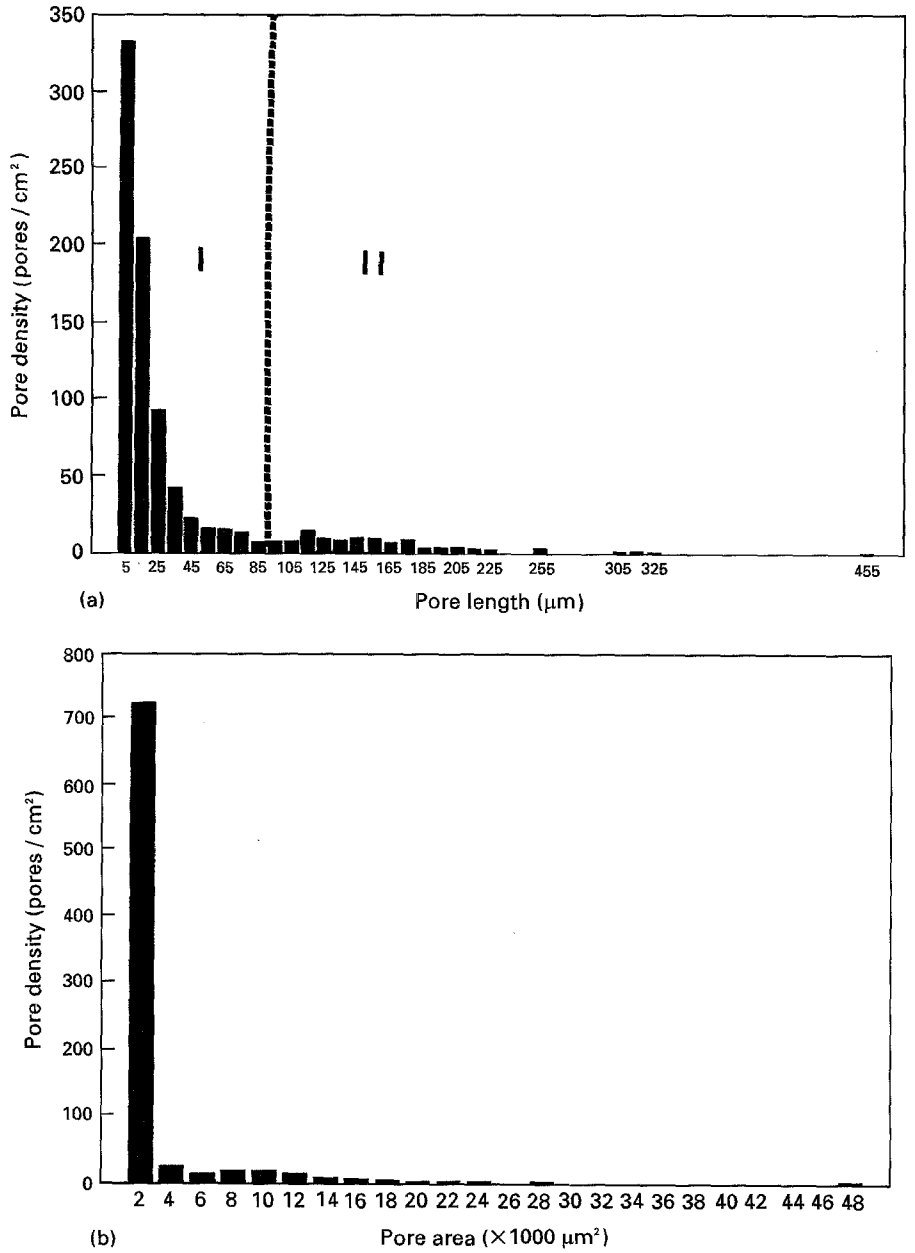

Figure 3 Distribution of pore density as a function of (a) pore length, and (b) pore area for a given sample.

where

$$\theta = \frac{1}{\sigma} = \frac{1}{\mu} \tag{2}$$

The results are displayed in Fig. 5 (a).

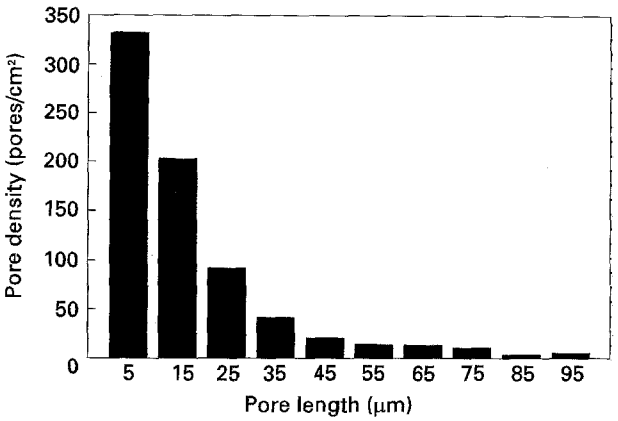

Figure 4 Exponential part of the pore length distribution curve for the sample shown in Fig. 3(a).

The fraction (density) of all pores that fall in a range of lengths between l_1 and l_2 can be calculated as

$$F(l_1, l_2) = \int_{l_1}^{l_2} \theta e^{-\theta l} dl \tag{3}$$

$$F(l_1, l_2) = [-e^{\theta l}]_{l_1}^{l_2} \tag{4}$$

$$F(0, l_{lim}) \sim 1 \tag{5}$$

The probable density of pores can be calculated by multiplying the probability function, f(l), by pore density in the exponential part, d_{exp} (Fig. 5(a)), giving

$$f(l) = \frac{d_{exp}}{\mu} e^{-1/\mu} \tag{6}$$

The density of pores found between l_1 and l_2 is then given by

$$F(l_1, l_2) = [-d_{exp} e^{-1/\mu}]_{l_1}^{l_2} \tag{7}$$

The measured and calculated exponential distributions of pore length are shown in Fig. 5(b).

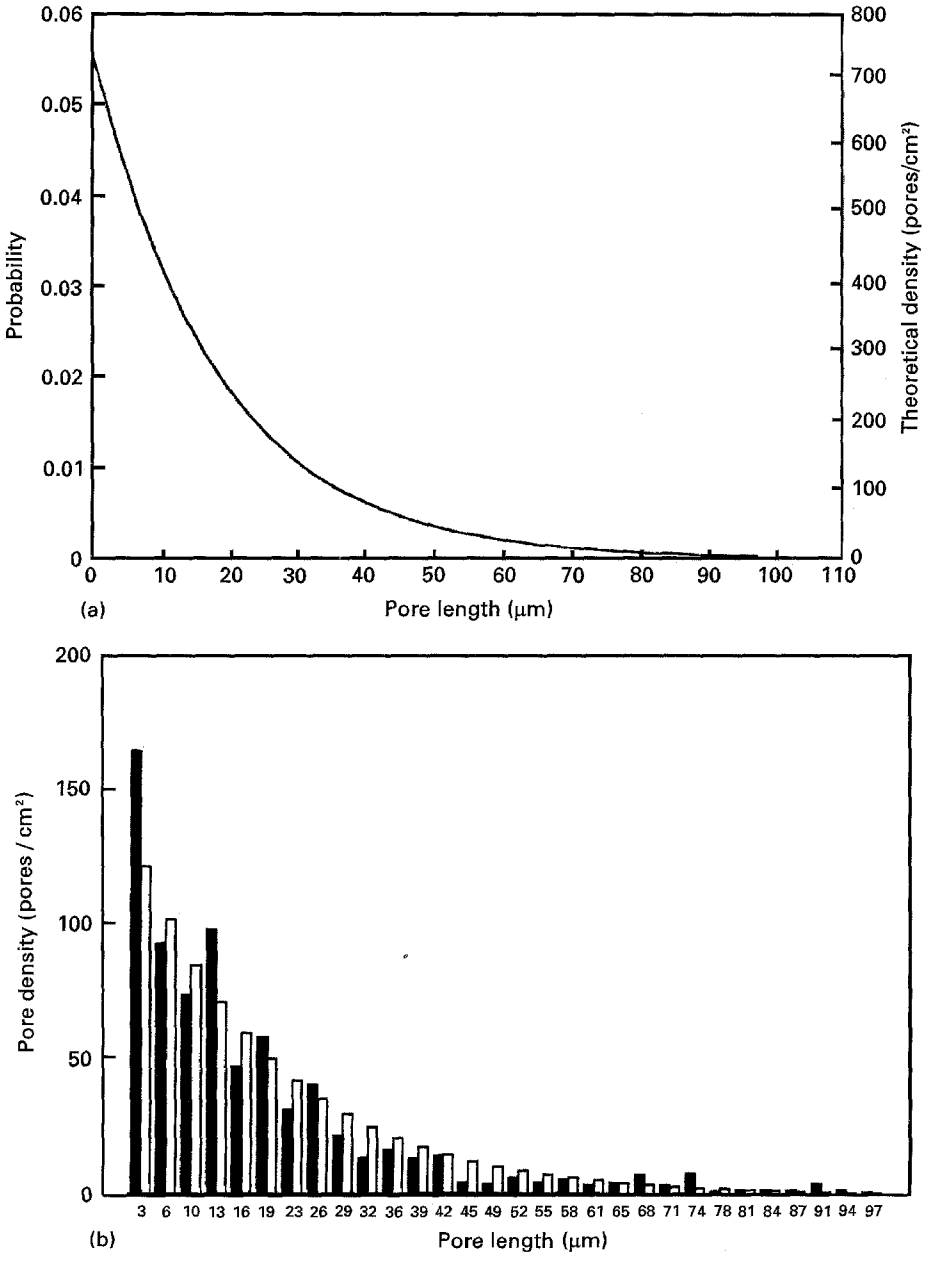

Figure 5 (a) Theoretical probability and calculated distribution of pore density as a function of pore length. (b) Experimental (■) and calculated (□) distribution of pore density as a function of pore length for the exponential part.

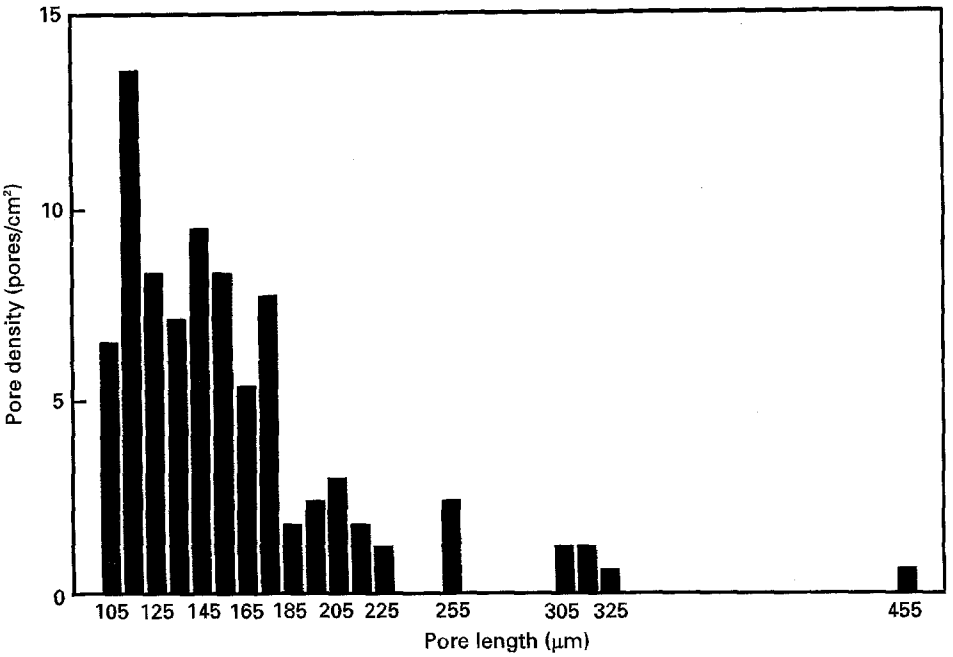

Figure 6 The irregular part of the pore length distribution curve for the sample shown in Fig. 3(a).

For pore lengths greater than l_{lim}, the distribution does not seem to obey a certain rule (Fig. 6). In this case, the law of uniform distribution is used, where the probability function for $l_{lim} \leq 1 \leq l_{max}$ is equal to a constant. Thus

$$f(l) = \frac{1}{l_{max} - l_{lim}} \tag{8}$$

where l_{max} is the maximum pore length, and l_{lim} is the limiting pore length.

In reality, $f(l)$ is not constant for all pores in the range l_{lim} to l_{max}. Thus

$$f(l) = \frac{d_c}{l_c d_{irr}} \tag{9}$$

where d_c is the density of a class, l_c is the length of the class and d_{irr} is the total density of the irregular part (Fig. 7(a)).

In order to calculate the fraction of all pores falling in the range l_1 and l_2 where $l_{lim} \leq l_1, l_2 \leq l_{max}$

$$F(l_1, l_2) = \int_{l_1}^{l_2} f(l)\,dl \tag{10a}$$

$$\text{and } F(l_1, l_2) = \int_{l_1}^{l_2} \frac{1}{l_{max} - l_{lim}}\,dl \tag{10b}$$

Thus,

$$F(l_1, l_2) = \frac{l_2 - l_1}{l_{max} - l_{lim}} \tag{11}$$

Fig. 7(b) compares the measured and calculated densities of pore length for the irregular part of the curve. As can be seen, the calculated values are significantly different from the measured ones. Practically, however, the exact distribution of pores in this part is not required. What is more important in determining the mechanical properties, particularly the alloy ductility, is the maximum value of pore length or pore area.

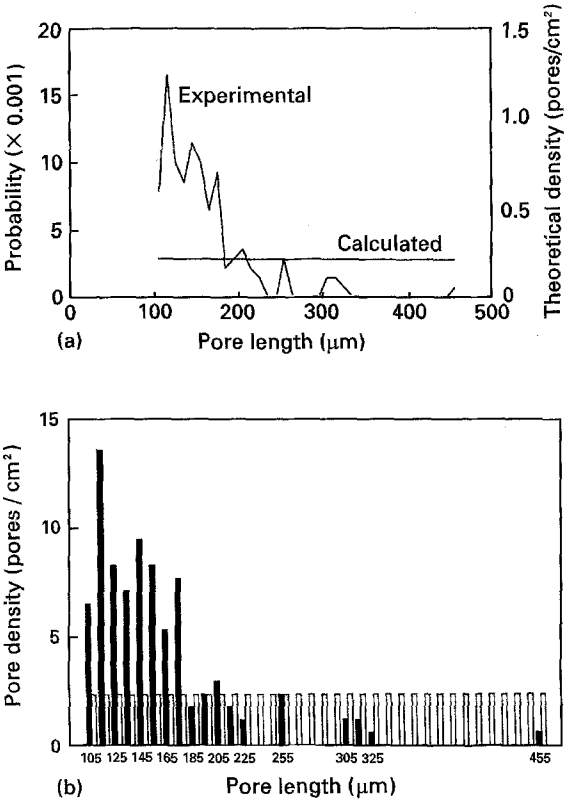

Figure 7 (a) Experimental versus calculated probability of pore density as a function of pore length. (b) Experimental (■) versus calculated (□) probability of pore density as a function of pore area.

The measured values from small (S) and large (L) samples (covering the entire solidification range investigated in the present study) for percentage of surface porosity (equivalent to approximately 0.85% of the porosity volume fraction [26]), pore area, pore length, and pore density are listed in Tables V–VIII, respectively.

TABLE V Percentage surface porosity measured for small (S) and large (L) samples obtained from various alloy castings

Alloy sample	Surface porosity (%)	Alloy Sample	Surface porosity (%)
f1S	0.451	h5S	1.83
f1L	1.16	h5L	2.835
f2S	0.236	h6S	0.145
f2L	0.444	h6L	0.218
f3S	0.068	h7S	0.032
f3L	0.269	h7L	0.114
f4S	0.152	h8S	1.804
f4L	0.513	h8L	2.522
f5S	0.280	s1S	0.061
f5L	0.813	s1L	0.68
f6S	0.611	s2S	0.366
f6L	1.506	s2L	1.308
f7S	0.207	s3S	0.021
f7L	0.730	s3L	0.2466
f8S	0.260	s4S	0.062
f8L	0.396	s4L	0.282
h1S	0.064	s5S	0.358
h1L	0.094	s5L	1.285
h2S	1.99	s6S	0.042
h2L	2.433	s6L	0.624
h3S	2.25	s7S	0.11
h3L	3.066	s7L	0.675
h4S	0.044	s8S	0.060
h4L	0.065	s8L	0.389

S samples: $t_s \sim 12.5$ s, L samples: $t_s \sim 71$ s.

3.3. Statistical calculations

In the present investigation, the independent variables or controlling parameters are the compositions of the alloying elements Zn, Fe, Mg, Mn, Ti, Sr and P, the grain refiner content, the hydrogen level and the two thermal parameters of solidification time and solidus velocity. The dependent variables or the porosity parameters are the surface porosity (i.e. cross-sectional porosity area measured across the sample surface by the image analyser), the densities corresponding to the exponential and irregular parts of the pore length and pore area distribution curves, the mean pore length and mean pore area observed in the two parts (i.e. exponential and irregular) of the two curves, the limiting values of pore length and pore area, as well as the maximum pore length and maximum pore area.

The aim of the statistical study is to define the importance of each of the controlling parameters on the porosity. In this respect, the effects of each of the independent variables is determined as well as those of the interactions (between these variables) considered strong enough to affect the porosity.

The two methods selected were the factorial method and the method of multiple regression analysis. They will be discussed separately in the sections that follow. A comparison of the results obtained from the two methods is given at the end.

3.3.1. Factorial method

The linear effect of an independent variable x on a dependent variable y is given by

$$y = C_1 + C_2 x \tag{12}$$

where C_1 and C_2 are coefficients.

TABLE VI Average and maximum pore areas for small (S) and large (L) samples obtained from the alloy castings prepared in the present work

Alloy Sample	Pore density versus pore area distribution curve			
	Exponential part		Irregular part	
	Average pore area (μm^2)	Maximum pore area (μm^2)	Average pore area (μm^2)	Maximum pore area (μm^2)
f1S	54.00	258.0	4902.0	22601.0
f1L	74.75	305.0	15913.0	57630.0
f2S	66.00	258.0	4666.0	142348.0
f2L	67.00	321.0	8988.0	105665.0
f3S	54.00	271.0	741.0	3465.0
f3L	72.0	341.0	1963.0	27501.5
f4S	64.00	291.0	1213.0	11061.0
f4L	58.0	248.0	4245.5	101841.5
f5S	67.0	248.0	3085.0	35277.0
f5L	99.0	434.0	6753.0	83270.0
f6S	50.0	250.0	7200.0	48148.0
f6L	64.00	281.0	13837.0	69324.0
f7S	66.4	300.0	1581.0	24958.0
f7L	70.0	316.0	3747.5	85184.5
f8S	55.0	769.0	2093.0	32216.0
f8L	81.0	352.0	2831.0	27099.5
h1S	65.0	271.0	972.0	6087
h1L	85.5	354.0	1525.0	7851.5
h2S	52.00	219.0	8781.0	83819.0
h2L	66.5	343.0	23991.5	397341.5
h3S	58.0	248.0	15847.0	83911.0
h3L	62.0	259.5	43615.0	153917.0
h4S	50.5	248.0	644.0	3588.0
h4L	63.5	284.0	1449.0	26390.0
h5S	66.0	271.0	13522.0	105494.0
h5L	63.0	310.0	25369.5	50471.5
h6S	59.5	248.0	1218.0	11704.0
h6L	73.00	321.0	1796.0	45827.5
h7S	49.5	250.0	486.0	1821.0
h7L	61.0	331.0	921.0	5556.0
h8S	57.5	269.0	7837.0	45750.0
h8L	57.5	281.0	15186.0	39448.9
s1S	83.00	321.0	2620.0	23170.0
s1L	120.0	286.0	9860.0	58302.0
s2S	64.00	283.0	3784.0	20042.0
s2L	75.0	341.0	14406.0	69706.0
s3S	42.0	196.0	507.0	2512.0
s3L	98.0	364.0	2169.0	29277.0
s4S	78.5	331.0	2497.0	26458.0
s4L	67.5	305.0	4011.0	26168.0
s5S	63.0	279.0	3178.0	26561.0
s5L	66.5	469.0	8352.0	89648.5
s6S	67.00	248.0	2320.0	13399.0
s6L	106.5	429.0	6813.5	217915.5
s7S	58.0	227.0	1515.0	18011.0
s7L	89.5	372.0	4191.5	12790.4
s8S	52.0	239.0	918.0	5036.0
s8L	70.0	290.2	2679.0	48989.0

If x^+ and x^- represent the maximum and minimum values of x, and with the aid of the following notations

$$y_1 = y(x^-); \quad y_2 = y(x^+) \tag{13}$$

$$\bar{y} = \frac{y_1 + y_2}{2} \text{ and } \Delta y = \frac{y_2 - y_1}{2} \tag{14}$$

$$\bar{x} = \frac{x^+ + x^-}{2} \text{ and } \Delta x = \frac{x^+ - x^-}{2} \tag{15}$$

the linear part may be written as:

$$y = \bar{y} + \Delta y \frac{x - x^-}{\Delta x} \text{ or } y = \bar{y} + e \frac{x - x^-}{\Delta x} \tag{16}$$

TABLE VII Average and maximum pore lengths for small (S) and large (L) samples obtained from the alloy castings prepared in the present work

Alloy Sample	Pore density versus pore length distribution curve			
	Exponential part		Irregular part	
	Average pore length (μm)	Maximum pore length (μm)	Average pore length (μm)	Maximum pore length (μm)
f1S	16.7	73.9	122.0	209.0
f1L	22.07	98.3	185.5	376.5
f2S	18.8	86.8	150.0	598.0
f2L	18.62	104.5	198.5	619.0
f3S	15.2	103.0	135.0	135.0
f3L	17.75	116.0	181.0	278.0
f4S	18.70	106.0	137.0	203.0
f4L	18.8	115.0	213.0	657.5
f5S	21.6	90.0	143.0	286.0
f5L	24.75	129.0	175.5	522.6
f6S	16.8	83.9	154.0	323.0
f6L	18.5	103.0	215.5	437.0
f7S	20.4	100.0	157.0	296.0
f7L	18.76	113.0	195.0	627.0
f8S	15.6	103.0	158.0	367.0
f8L	21.7	119.0	169.0	283.0
h1S	19.2	123.0	173.0	184.0
h1L	18.1	110.0	188.0	248.0
h2S	21.6	90.3	175.0	458.0
h2L	19.85	98.3	216.0	371.0
h3S	21.1	93.3	229.0	431.0
h3L	16.95	107.7	321.0	675.0
h4S	14.4	103.0	–	–
h4L	17.0	109.5	183.0	424.0
h5S	18.6	106.0	224.0	468.0
h5L	17.75	119.0	357.0	691.0
h6S	17.9	113.0	147.0	199.0
h6L	18.85	120.5	219.0	527.0
h7S	12.9	87.1	–	–
h7L	16.75	98.3	129.0	213.0
h8S	19.9	93.3	175.0	386.0
h8L	18.05	105.0	247.0	703.0
s1S	27.3	113.0	179.0	235.0
s1L	29.2	146.5	245.0	338.0
s2S	21.5	88.5	127.0	192.0
s2L	21.3	119.0	217.0	408.0
s3S	12.9	90.0	–	–
s3L	26.7	171.0	198.5	373.0
s4S	19.7	116.0	215.0	215.0
s4L	19.0	99.8	159.0	399.0
s5S	22.5	103.0	158.0	273.0
s5L	24.5	103.0	185.0	454.5
s6S	24.5	113.0	141.0	141.0
s6L	26.35	169.0	290.0	344.0
s7S	19.0	100.0	173.0	350.0
s7L	21.8	154.0	217.0	514.0
s8S	15.7	90.3	144.0	200.0
s8L	20.8	123.0	182.0	395.0

TABLE VIII Average pore density (number of pores/cm^2) for small (S) and large (L) samples obtained from the alloy castings prepared in the present work

Alloy Sample	Pore density versus pore length distribution curve		Pore density versus pore area distribution curve	
	Exponential part	Irregular part	Exponential part	Irregular part
f1S	213.0	58.4	101.0	90.1
f1L	239.5	68.1	199.1	108.4
f2S	208.0	11.3	171.1	48.1
f2L	372.0	23.05	315.0	79.55
f3S	575.0	1.0	469.0	57.3
f3L	842.5	11.25	746.0	108.0
f4S	552.0	10.2	461.0	101.0
f4L	601.0	30.7	493.0	138.0
f5S	295.0	22.5	231.0	86.0
f5L	414.5	50.7	344.0	121.5
f6S	173.0	52.2	141.0	83.9
f6L	244.0	57.85	206.0	96.5
f7S	534.0	14.3	436.0	113.0
f7L	787.0	39.0	644.0	179.0
f8S	794.0	18.4	707.0	105.0
f8L	648.0	76.1	540.0	134.0
h1S	271.0	2.0	225.0	48.1
h1L	182.0	10.2	176.0	31.75
h2S	641.0	173.0	476.0	33.0
h2L	388.5	116.5	327.0	178.0
h3S	255.0	86.0	203.0	138.0
h3L	245.0	57.85	210.0	91.75
h4S	362.0	–	319.0	43.0
h4L	363.0	9.2	319.5	48.1
h5S	422.0	63.5	351.0	134.0
h5L	490.5	56.3	421.0	126.0
h6S	539.0	10.2	453.0	97.3
h6L	544.5	14.3	473.5	78.3
h7S	340.0	–	305.0	34.8
h7L	555.0	16.4	495.0	85.0
h8S	488.0	135.0	396.0	227.0
h8L	492.5	127.5	414.0	167.0
s1S	65.0	2.3	45.5	21.9
s1L	346.5	26.6	265.5	107.35
s2S	247.0	36.2	197.0	86.7
s2L	390.0	72.15	326.0	136.5
s3S	193.0	–	166.0	27.6
s3L	358.5	10.5	288.5	82.5
s4S	128.0	1.0	107.0	21.5
s4L	429.0	24.6	377.0	76.8
s5S	336.0	26.6	255.0	107.0
s5L	303.5	65.0	231.0	137.5
s6S	69.6	1.0	54.3	16.4
s6L	328.6	30.0	265.0	92.0
s7S	762.0	7.2	205.0	64.5
s7L	636.5	22.5	510.5	148.5
s8S	330.0	6.1	787.0	49.1
s8L	576.0	73.5	471.0	128.5

where the effect (e) of x on y is given by

$$e = \Delta y \tag{17}$$

Following a similar analysis, the linear equation for three independent variables (x_1, x_2, x_3) and their interactions is given by

$$y = C_1 + C_2x_1 + C_3x_2 + C_4x_3 + C_5x_1x_2 + C_6x_1x_3 + C_7x_2x_3 + C_8x_1x_2x_3 \tag{18}$$

In this case, eight (2^3) experiments are required to be able to determine the eight coefficients (where the three independent variables are assigned their maximum (+) or minimum (−) values). Therefore

$$y = \bar{y} + e_{x_1}\frac{x_1 - \bar{x}_1}{\Delta x_1} + e_{x_2}\frac{x_2 - \bar{x}_2}{\Delta x_2} + e_{x_3}\frac{x_3 - \bar{x}_3}{\Delta x_3} + e_{x_1x_2}\frac{(x_1 - \bar{x}_1)(x_2 - \bar{x}_2)}{\Delta x_1 \Delta x_2} + e_{x_1x_3}\frac{(x_1 - \bar{x}_1)(x_3 - \bar{x}_3)}{\Delta x_1 \Delta x_3}$$

$$+ e_{x_2x_3} \frac{(x_2 - \bar{x}_2)(x_3 - \bar{x}_3)}{\Delta x_2 \Delta x_3}$$

$$+ e_{x_1x_2x_3} \frac{(x_1 - \bar{x}_1)(x_2 - \bar{x}_2)(x_3 - \bar{x}_3)}{\Delta x_1 \Delta x_2 \Delta x_3} \quad (19)$$

Each effect can be calculated by taking the average of the eight results multiplied by their respective signs (+ or −). For example, the effect of the interaction x_1x_3 can be calculated as

$$e_{x_1x_3} = \frac{y_1 - y_2 + y_3 - y_4 - y_5 + y_6 - y_7 + y_8}{8} \quad (20)$$

As mentioned earlier, an examination of the controlling parameters and their interactive effects led to regrouping these variables into three groups of four variables each, namely, the iron, strontium and hydrogen groups. Normally, therefore, one would require 16 (2^4) experiments to be able to measure all the effects of these parameters and their interactions. However, it is possible to use a model of three variables instead, if one supposes that the effect of the interaction $x_1x_2x_3$ in the latter is negligible. That is, one measures the effect of a fourth element x_4 that represents or is "confounded" with the $x_1x_2x_3$ interaction. One thus obtains a confound model for four variables based on the model for three variables described previously.

Following such a method of analysis (complete details of which are to be found in [27]), the results obtained for the dominant effects and interactions could be expressed in terms of a relative effect e_{rel} (as a percentage) given by

$$e_{rel} = \frac{e}{\bar{y}} \quad (21)$$

The calculated relative effects for the three groups are shown in Table IX(a)–(c) for the thirteen dependent variables given in column 1 in each table. To obtain a better idea of the importance of the relative effects reported in these tables, the results are regrouped in Table X, where a relative effect below 20% is considered negligible, between 20 and 50% as slight, and at higher percentages as significant.

3.3.2. Multiple regression method

In the multiple regression method, applied to the 72 solidification experiments that were performed, significant terms of the regression were selected using the stepwise reduction method. Table XI lists all possible variables and interactions involved, including the solidus velocity (V_s) and local solidification time (t_s), giving 11 simple variables, 28 interaction products, and 9 supplementary confound variables (the latter are used when for a given observed data, a satisfactory equation cannot be obtained using the 39 (11 + 28) initial variables).

For an appropriate choice of the regression equation, the factor of multiple regression R^2, the condition number N, and the T-value of each variable should be taken into consideration. The R^2 value allows for adjusting the regression equation between an independent (predictor) and a dependent (response) variable.

TABLE IX (a) Relative effects (e_{rel}) for the iron group (%)

Dependent variables	Mn	Fe	Zn	P	Mn–Fe	Fe–P	Mn–P
All pores							
Surface porosity	−1	−71	32	−62	6	35	−1
Exponential part of pore length distribution curve							
Density	−10	85	8	21	−2	−3	2
Limiting length	1	14	1	4	−0	−4	−4
Average length	−6	−3	7	−1	7	−7	5
Irregular part of pore length distribution curve							
Density	−17	−79	31	−66	27	37	11
Maximum length	25	−20	−1	−1	−14	−45	16
Average length	8	−1	2	−7	−6	−4	−2
Exponential part of pore area distribution curve							
Density	−10	87	5	24	−4	1	1
Limiting area	−6	4	5	5	3	−3	4
Average area	−5	−0	5	4	6	−6	6
Irregular part of pore area distribution curve							
Density	−11	27	24	−19	12	−8	9
Maximum area	34	−58	−8	1	−21	−58	20
Average area	18	−102	13	−54	−5	37	−3

TABLE IX (b) Relative effects (e_{rel}) for the hydrogen group (%)

Dependent variables	GR	P	Mg	H	Mg–H	P–H	GR–H
All pores							
Surface porosity	15	−24	−32	187	−36	−21	12
Exponential part of pore length distribution curve							
Density	27	−6	44	3	−14	−18	3
Limiting length	−1	−9	2	−5	6	5	−9
Average length	6	−10	−4	10	−2	6	3
Irregular part of pore length distribution curve							
Density	59	−16	−22	180	−28	−13	58
Maximum length	−2	−17	9	109	7	−1	−17
Average length	−13	−12	−2	57	3	11	−19
Exponential part of pore area distribution curve							
Density	26	−4	45	−1	−13	−18	0
Limiting area	2	−9	1	−2	2	0	2
Average area	−1	−14	−2	−1	4	7	−2
Irregular part of pore area distribution curve							
Density	48	−17	5	98	−24	−16	36
Maximum area	−34	−54	8	179	4	−46	−45
Average area	−40	−2	−27	176	−27	4	−43

It gives the proportion of the variation in the value of the dependent variable with respect to its average.

The condition number N, evaluates the collinearity between the independent variables. Its value varies between one and infinity. A value of one indicates a matrix of perfect orthogonal independent variables. High N levels (50–100) show that the model contains collinear terms.

TABLE IX (c) Relative effects (e_{rel}) for the strontium group (%)

Dependent variables	Ti	Mg	Zn	Sr	Ti–Mg	Mg–Sr	Ti–Sr
All pores							
Surface porosity	9	−100	22	36	−16	−64	11
Exponential part of pore length distribution curve							
Density	12	22	38	8	−5	−4	14
Limiting length	−4	−7	4	−18	−9	16	−4
Average length	−8	−21	−1	−12	4	10	2
Irregular part of pore length distribution curve							
Density	17	−100	8	82	−3	−95	26
Maximum length	2	−10	25	−16	−7	−16	4
Average length	2	−10	7	−19	−4	4	−0
Exponential part of pore area distribution curve							
Density	17	27	36	9	−5	−4	15
Limiting area	3	−15	−7	−20	4	11	1
Average area	−2	−17	−5	−24	2	16	1
Irregular part of pore area distribution curve							
Density	−1	−25	38	23	−7	−28	14
Maximum area	10	−56	34	−50	−26	−21	−1
Average area	13	−83	−7	6	−4	−41	11

The T-value of a variable is the value associated with the coefficient of a predictor parameter divided by its standard deviation. It is used to test if the true value of the coefficient is zero. It follows the degree of freedom rule, $n - k - 1$, where n is the number of experiments in the present work (24 castings × 3 specimens), and k is the number of variables in the model. The threshold value, T_{th}, for a certain level of significance, α, indicates that the variable is significant for the model when $|T| > T_{th}$. The higher the value of T for a certain variable, the more important the variable is for the model.

The software used in the present work, commercially known as RS-1, is based on the stepwise regression method [23]. The T-value of each independent variable is the main element for such a technique. This regression method essentially involves introducing or removing, successively, the independent variables one at a time, according to certain criteria related to their level of significance. The selection of parameters is completed when no more independent variables can be added to, or subtracted from, the regression model. For example, percentage porosity can be expressed as [2]

$$\% \text{ porosity} = A[\text{H}]^2 + B([\text{H}] \times t_f) + C([\text{Sr}] \times [\text{H}]) + D(\text{GR}) + \ldots$$

where [H] is the hydrogen content, [H] × t_f is the hydrogen content multiplied by the solidification time (an interaction term), [Sr] × [H] is a Sr times hydrogen level interaction, and $A, B, C, \ldots$ are the fitted coefficients.

The calculated T-values for the eight dependent variables of our study (surface porosity, and the

TABLE X Interpretation of relative effects (e_{rel}) obtained for the three groups, calculated using the factorial method

Element or interaction	Surface porosity	Exponential part of pore length/pore area distribution curve	Irregular part of distribution curve					
			Pore length			Pore area		
		Pore density	Density	Average	Maximum	Density	Average	Maximum
Zn	+	+				+		
Fe	− −	+ +	− −		−	+	− −	− −
Mg	− −	+	− −				− −	−
Mn					+			+
Ti								
Sr	+ +		+ +			+		− −
P	−		−				−	−
GR		+	+ +			+	−	−
H	+ +		+ +	+ +	+ +	+ +	+ +	+ +
Fe–Mn			+					−
Fe–P	+		+		−		+	− −
Mn–P								+
H–P	−							−
H–Mg	−		−			−		−
H–GR			+ +			+	−	−
Mg–Sr	− −		− −			−	−	−
Sr–Ti			+					
Mg–Ti								−

− −: Significant reduction; −: slight reduction;
+ +: significant increase; +: slight increase.

densities and maximum and average values of the pore length and pore area obtained from the exponential and irregular parts of the respective distribution curves) are listed in Table XII. The t_{th} value at a level of significance $\alpha = 0.005$ is approximately 1.96. A regression equation is said to give a good evaluation of the dependent variables when $N < 10$ and $R^2 > 0.7$. It is evident from Table XII that the percentage surface porosity is the most significant parameter from a statistical standpoint. Fig. 8 depicts a good distribution of the uncertainty residuals. Other parameters that could be evaluated with an acceptable level of confidence were the maximum pore length, pore area, and areal pore density for the irregular part of the distribution curves.

It was not possible, however, to improve the statistical fitness of the model to predict the other response variables with confidence. The importance of the marginal contributions shown in Table XII is expressed in Table XIII, similar to that shown for the case of the relative effects in Table X.

TABLE XI Independent (predictor) variables obtained from the regression method

Initial variables				Supplementary (confound) variables
Simple variables	Interactions between constituents	Interaction with t_s	Interaction with V_s	
Fe	Fe–P	Fe–t_s	Fe–V_s	Zn–P
Sr	Fe–Mn	Sr–t_s	Sr–V_s	Mn–Zn
H	P–Mn	H–t_s	H–V_s	Fe–Zn
Mg	H–Mg	Mg–t_s	Mg–V_s	GR–Mg
P	H–P	P–t_s	P–V_s	GR–P
Zn	H–GR	Zn–t_s	Zn–V_s	P–Mg
Mn	Sr–Mg	Mn–t_s	Mn–V_s	Zn–Sr
Ti	Sr–Ti	Ti–t_s	Ti–V_s	Ti–Zn
GR	Mg–Ti	GR–t_s	GR–V_s	Mg–Zn
t_s	t_s–V_s	–	–	–
V_s	–	–	–	–

t_s: local solidification time.
V_s: solidus velocity.

3.3.3. Presentation of the data

In this section, results obtained from the regression method are presented in the form of contour plots to emphasize the interaction effect of two elements on pore size and density. It can be seen from Tables IX (factorial method) and XII (regression method) that hydrogen is the strongest element contributing to all the eight response parameters. However, while the factorial method shows that the hydrogen–magnesium (H–Mg) interaction slightly reduces the percentage surface porosity, density of pore length, and area of the irregular part of the curve, the regression method reveals an effect to the contrary, as displayed in Fig. 9.

According to the factorial method, the hydrogen–grain refiner (H–GR) interaction has an important

TABLE XII T-values for the dependent (response) variables, obtained from the regression method

Element or Interaction	Surface porosity	Exponential part of pore length distribution curve			Irregular part of pore length/pore area distribution curve			
		Pore length			Pore length		Pore area	
		Density	Average	Maximum	Density	Average	Density	Maximum
N	9.3	2.2	17.3	18.3	17.9	8.8	8.1	10.7
R^2	0.83	0.67	0.27	0.67	0.86	0.64	0.59	0.69
constant	– 5.7	1.6	37.8	24.6	– 4.2	24.2	4.7	19.9
H	14.5				9.2	7.3		6.1
H–P	– 4.6				– 5.8		– 3.3	
H–GR	5.7	2.4			7.8		4.8	
Mg–Sr	– 3.8	– 2.6		– 5.1	– 6.5			– 3.9
Mg–Ti		– 1.7	2.3		4.1			
Zn–P					3.6	2.1	2.7	
Fe–P						3.1		– 2.5
GR–V_s					4.8	2.7	4.3	3.6
t_s–V_s	6.9	4.3	2.4			6.6		6.0
Fe		7.7						
Mg		3.4	– 3.1	4.6				
Zn				3.1				
Ti			– 2.7					
Sr					6.0			
GR					– 3.5			
V_s		3.3						
t_s				– 8.3				
H–Mg								2.4
H–Sr				2.5				
H–V_s							5.6	
H–t_s					– 4.6			
Fe–V_s				– 3.4	– 4.2			
Mg–P				3.4				
Ti–P				– 5.7				
Ti–t_s				5.0				
Zn–V_s				3.8				
Sr–P				4.4				

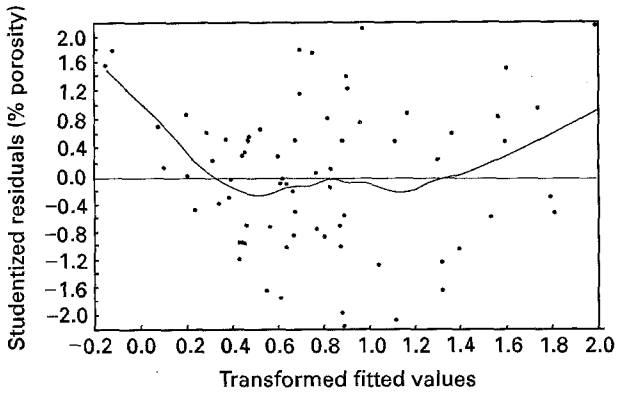

Figure 8 Distribution of residuals of uncertainty.

TABLE XIII Interpretation of calculated variation in the dependent variables, using the regression method

Independent variables	Surface porosity	Irregular part of distribution curve		
		Pore length	Pore area	
		Maximum	Density	Maximum
constant	− −	+ +	+	+ +
H	+ +	+ +		+ +
H–P	−		−	
H–GR	+ +		+	
Mg–Sr	−			−
Zn–P		+	+	
Fe–P		−		−
GR–V_s		+	+	+
t_s–V_s	+ +	+ +		+ +
H–Mg				+
H–V_s			+ +	

− −: significant reduction; −: slight reduction;
+ +: significant increase; +: slight increase.

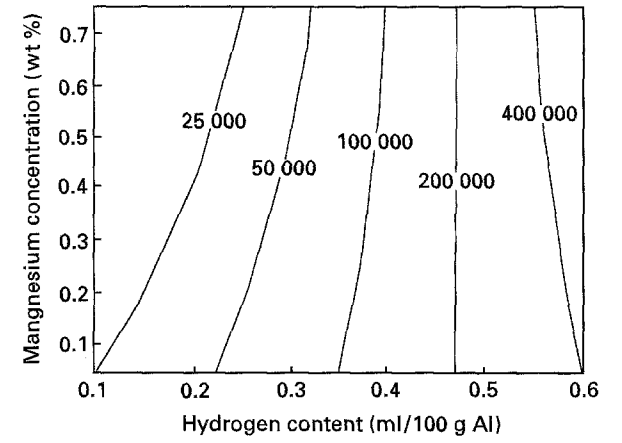

Figure 9 Contour plot of maximum pore area (μm²) as a function of hydrogen and magnesium concentrations.

effect on increasing the areal pore density and pore length. However, this interaction slightly reduces the maximum and average pore area. In confirmation of these findings, the regression model also shows that the H–GR interaction markedly enhances the increase in percentage of surface porosity (Fig. 10) and areal pore density (Table XII).

The regression method highlights the important role of the hydrogen–solidus velocity (H–V_s) interaction in increasing the areal pore density, compared to the grain refiner–solidus velocity (GR–V_s) interaction that has a reduced effect on the same. The latter is demonstrated in Fig. 11. Both methods confirm that strontium (Sr) has a strong effect on porosity formation, whereas magnesium (Mg) has an opposite effect. Apparently, the Sr–Mg interaction leads to a drastic decrease in pore size and percentage of surface porosity as seen in Fig. 12, in good agreement with the predictions of the factorial method.

As can be noted from Table XIII, hydrogen reinforces porosity formation at all levels of solidus velocity. The regression model predicts that increasing the local solidification time produces a similar trend, though with a different magnitude, as illustrated in Fig. 13.

Table XIV compares the global effect of the different independent variables (alloying elements, additives, and their interactions) on porosity formation (pore density and size) in Al–Si–Cu base alloys obtained by the two methods of calculation. It can be seen that the two methods arrive at the same predictions for only some of the independent variables, in

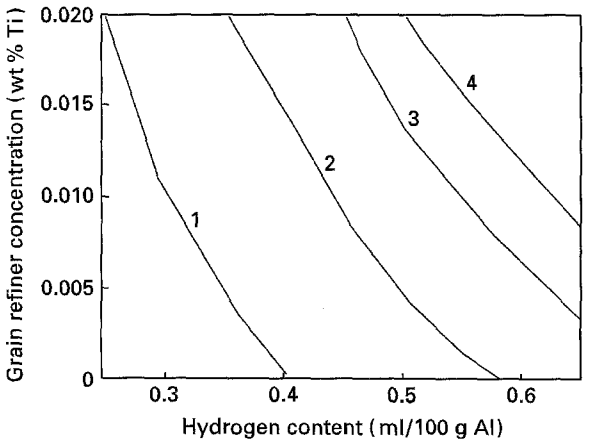

Figure 10 Contour plot of surface porosity (%) as a function of hydrogen and grain refiner (measured by Ti wt %) concentrations.

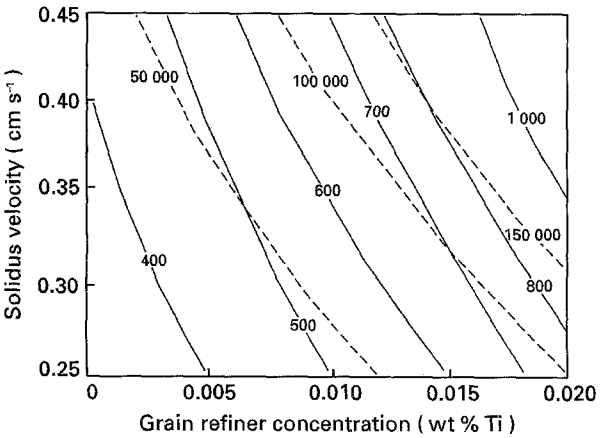

Figure 11 Contour plot of maximum pore length (μm, ——) and pore area (μm², -----) as a function of grain refiner concentration and solidus velocity.

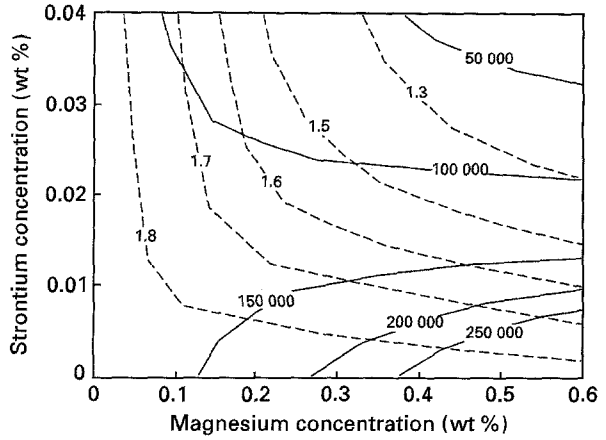

Figure 12 Contour plot of surface porosity (%, -----) and maximum pore area (μm², ———) as a function of magnesium and strontium concentrations.

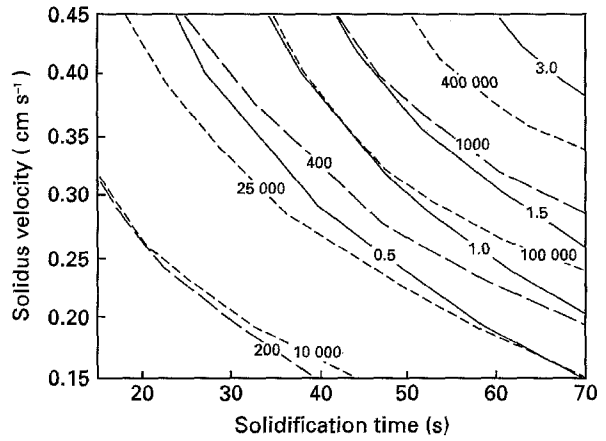

Figure 13 Contour plot of surface porosity (%, —), pore length (μm, ------), and pore area (μm², ...) as a function of local solidification time and solidus velocity.

TABLE XIV Influence of independent variables on porosity: comparison of results obtained from the factorial and regression methods

Variable (element or interaction)	Effect on porosity formation	
	Factorial method	Regression method
H	+ +	+ +
H–V_s	nil	+ +
H–Mg	−	+
H–GR	+ +	+ +
H–P	−	−
Zn	+	nil
Fe	−	nil
Mg	−	nil
Mn	+	nil
Ti	nil	nil
Sr	+ +	+ +
P	−	nil
GR	+	−
Fe–Mn	−	nil
Zn–P	+	nil
Fe–P	−	−
Mn–P	+	nil
Mg–Sr	− −	− −
Sr–Ti	+	+
Mg–Ti	−	nil
t_s–V_s	nil	+ +

+ +: Significant increase; +: slight increase;
− −: Significant reduction; −: slight reduction.

particular, hydrogen, hydrogen–grain refiner, hydrogen–phosphorus, strontium, iron–phosphorus, magnesium– strontium, titanium, and strontium–titanium (for details see Tables IX and XII).

Summary

1. Hydrogen is the strongest element/variable enhancing porosity formation. Its strength is reinforced by the presence of other parameters contributing to porosity formation, mainly strontium.

2. Both methods of statistical calculation, i.e. the factorial method and the multiple regression method, arrived at the following predictions:

(a) Hydrogen, hydrogen-grain refiner, strontium, strontium–titanium, as well as the solidus velocity–solidification time are variables that significantly enhance porosity formation and increase in pore size.

(b) Grain-refiner, hydrogen–phosphorus, strontium–magnesium, and iron–phosphorus variables reduce the porosity, although in differing magnitudes.

(c) Titanium is a neutral element.

3. The solidification time-solidus velocity (t_s–V_s) interaction can only be evaluated by means of the regression technique, where it is found that this interaction significantly increases the surface porosity and maximum pore length and area.

4. It is rather difficult to affirmatively establish the role of the other independent variables using one method without being contradicted by the other.

Appendix 1

Examples of the porosity features typically observed in alloy samples obtained under different conditions of solidification and containing varying hydrogen, strontium and grain refiner levels are shown in Fig. 14.

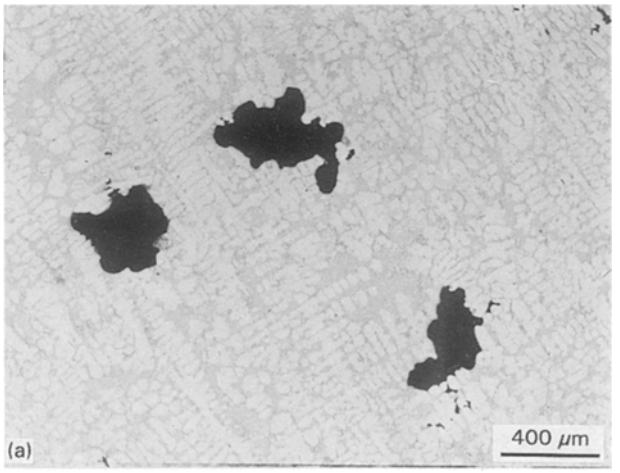

Figure 14 Micrographs displaying examples of the porosity features typically observed in alloy samples obtained under different conditions of solidification and containing varying hydrogen, strontium or grain refiner levels: (a) alloy sample h5L (H = 0.57 ml/100 g Al; $t_s \cong 71$ s); (b) alloy sample h6S (GR = 0.02 wt % Ti; $t_s \cong 12.5$ s); (c) alloy sample s1S (Sr = 0%; $t_s \cong 12.5$ s); (d) alloy sample s5L (Sr = 0.03 wt %; $t_s \cong 71$ s).

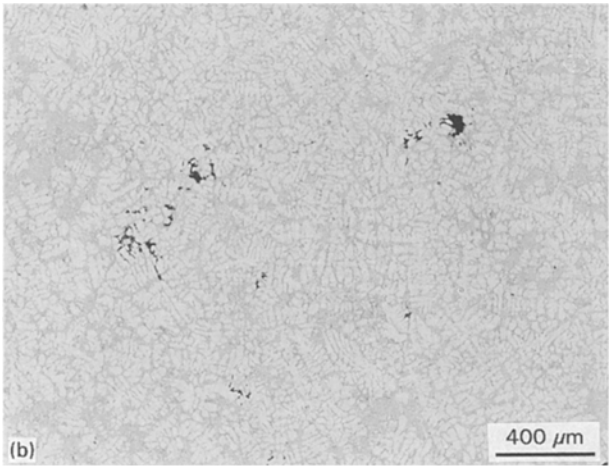

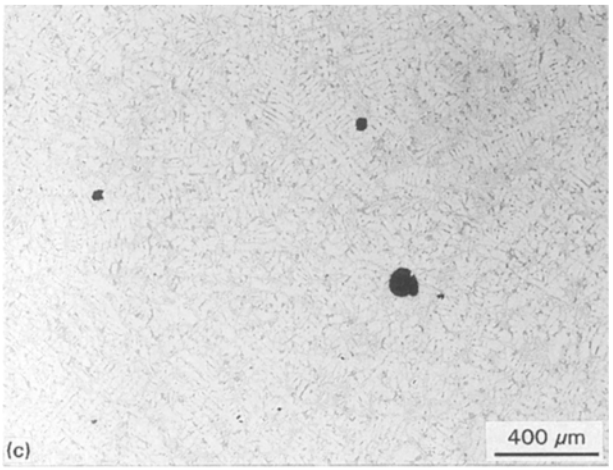

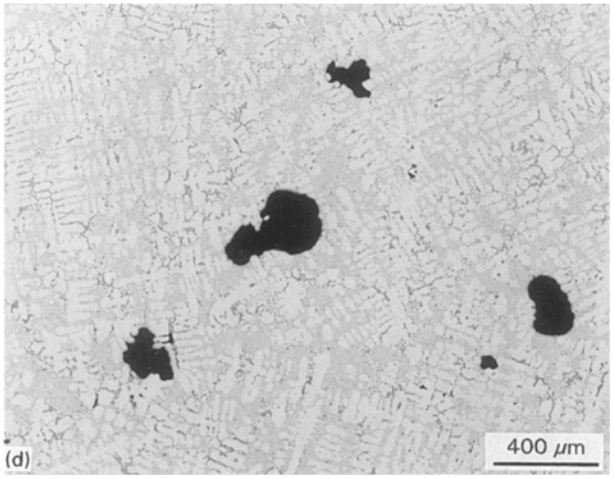

Figure 14 (continued).

The various dependent (response) variables or porosity parameters measured using an image analyser (in conjuction with an optical microscope) are defined as follows:

Surface porosity: porosity area percentage as measured by the image analyser for a specified area of sample surface (same for all samples).

Pore density: number of pores counted by the image analyser per unit area (cm^2) of the sample surface.

Pore area: area of a pore (μm^2) as determined by the image analyser.

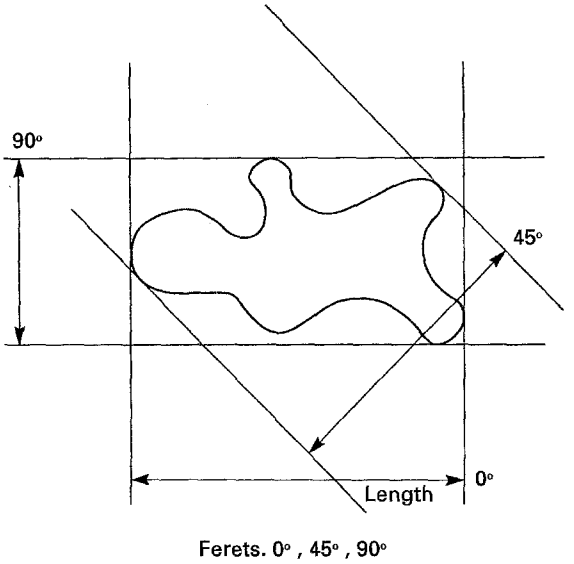

Figure 15 Schematic diagram showing ferets measured by the Leco 2001 image analyser for a typical pore, where the longest feret (at 0°) gives a measure of the pore length.

Pore length: longest of the ferets measured by the image analyser for a specific pore (ferets being the straight line measurements made between tangents at various angles on the specified feature (pore); the image analyser measures 8 ferets at 0°, 22.5°, 45°, 67.5°, 90°, 112.5°, 135° and 157.5° (see Fig. 15)).

Acknowledgements

The authors are indebted to Dr J. F. Major of Kingston Research and Development Centre, Alcan International Limited for his help with the regression analysis. They would like to thank Mr Lin Zhang, Department of Applied Sciences, Université du Québec à Chicoutimi, for his assistance with the experimental work, and Dr A. M. Samuel of the same department for a critical reviewing of the manuscript. Thanks are also extended to KB Alloys, Inc., Robards, KY, USA, for supplying the master alloys used in the present work. Financial support received from the Natural Sciences and Engineering Research Council of Canada, the Fondation de l'Université du Québec à Chicoutimi, and the Societe d'électrolyse et de chimie Alcan (SECAL) is gratefully acknowledged.

References

1. H. HUANG and J. T. BERRY, *Amer. Foundrymen's Soc. Trans.* **101** (1993) 669.
2. K. E. TYNELIUS, J. F. MAJOR and D. APELIAN, *Ibid.* **101** (1993) 401.
3. C. E. RANSLEY and H. NEUFELD, *J. Inst. Met.* **74** (1948) 599.
4. H. IWAHORI, K. YONEKURI, Y. SUGIYAMA, Y. YAMAMOTO and M. NAKAMURI, *Amer. Foundrymen's Soc. Trans.* **93** (1985) 443.
5. P. M. THOMAS and J. E. GRUZLESKI, *Metall. Trans. B* **9B** (1978) 139.
6. J. E. GRUZLESKI, P. M. THOMAS and R. A. ENTWHISTLE, *British Foundryman* **71** (1978) 69.

7. Y. W. LEE, E. CHANG and C. F. CHIEU, *Metall. Trans. B* **21B** (1990) 715.
8. *Idem., Mater. Sci. Engng.* **A124** (1990) 233.
9. W. D. WALTHER, C. M. ADAMS and H. F. TAYLOR, *Amer. Foundrymen's Soc. Trans.* **64** (1956) 658.
10. H. FREDRIKSSON and I. SVENSSON, *Metall. Trans. B* **7B** (1976) 599.
11. H. SHAHANI, *Scand. J. Metall.* **14** (1985) 306.
12. T. S. PIWONKA and M. C. FLEMINGS, *Trans. AIME* **236** (1966) 1157.
13. K. KUBO and R. D. PEHLKE, *Metall. Trans. B* **16B** (1985) 359.
14. Q. T. FANG and D. A. GRANGER, *Amer. Foundrymen's Soc. Trans.* **97** (1989) 989.
15. S. SHIVKUMAR, D. APELIAN and J. ZOU, *Ibid.* **98** (1990) 897.
16. J. D. ZHU and I. OHNAKA, in Modeling of Casting, Welding, and Advanced Solidification Technologies, Conference Proceedings, Davos, Switzerland, 1990.
17. K. E. TYNELIUS, Ph.D. Thesis, Drexel University, Philadelphia, PA, 1992.
18. C. E. RANSLEY, D. E. J. TALBOT and H. C. BARLOW, *J. Inst. Met.* **86** (1957–58) 212.
19. A. M. SAMUEL and F. H. SAMUEL, *J. Mater. Sci.* **27** (1992) 6533.
20. C. DUPUIS, Z. WANG, J.-P. MARTIN and C. ALLARD, *Light Metals* (1992) 1055.
21. A. M. SAMUEL and F. H. SAMUEL, *J. Mater. Sci.* **29** (1994) 3591.
22. N. ROY, L. ZHANG, P. R. LOUCHEZ and F. H. SAMUEL, *Ibid.* **31** (1996) 1243.
23. L. ANANTHA NARAYANAN, F. H. SAMUEL and J. E. GRUZLESKI, *Metall. Mater. Trans. A* **25A** (1994) 1761.
24. G. E. P. BOX, W. G. HUNTER and J. S. HUNTER (eds), "Statistics for experimentation" (J. Wiley and Sons, New York, 1978).
25. G. KEPPEL (ed.), "Design and analysis: a researcher's handbook" 3rd edn (Prentice-Hall, Inc., 1991).
26. J. ZOU, K. E. TYNELIUS, S. SHIVKUMAR and D. APELIAN, in "Production, refining, fabrication and recycling of light metals", edited by M. Bouchard and P. Tremblay (Pergamon Press, New York, 1990) p. 323.
27. N. ROY, M. Eng. Thesis, Université du Québec à Chicoutimi, 1995.
28. RS-Explore Statistical Appendices, BBN Software Products Corporation, Cambridge, MA, USA.

Received 8 December 1995
and accepted 15 January 1996